Journal of Nuclear Materials 390–391 (2009) 428–431

Contents lists available at ScienceDirect

Journal of Nuclear Materials

journal homepage: www.elsevier.com/locate/jnucmat

Comparison of edge plasma behavior at different poloidal positions in Heliotron J

T. Mizuuchi [a,*], K. Murai [b], S. Watanabe [b], S. Yamamoto [a], S. Kobayashi [a], K. Nagasaki [a], H. Okada [a], G. Motojima [b], H. Arimoto [b], F. Hamagami [b], D. Katayama [b], H. Matsuoka [b], A. Nakajima [b], H. Takahashi [b], H. Yasuda [b], K. Mukai [b], Y. Kowada [b], K. Hosaka [b], S. Mihara [b], N. Nishino [c], Y. Nakashima [d], Y. Nakamura [b], K. Hanatani [a], K. Kondo [b], F. Sano [a]

[a] Institute of Advanced Energy, Kyoto University, Gokasho, Uji 611-0011, Japan
[b] Graduate School of Energy Science, Kyoto University, Gokasho, Uji, Japan
[c] Graduate School of Engineering, Hiroshima University, Higashi-Hiroshima 739-8527, Japan
[d] Plasma Research Center, University of Tsukuba, Tsukuba, Ibaraki 305-8577, Japan

ARTICLE INFO

PACS:
52.55.Hc
52.70.Ds
52.25.Fi

ABSTRACT

The edge plasma profile (the ion-saturation current profile) and its time evolution at three different positions of the field topology (near inboard-X, outboard-O and outboard-X points) are discussed focusing on the spontaneous transition to an improved mode in Heliotron J ECH-plasma. For all three positions it is found that the plasma profile becomes steeper as progress of the transition. In the early phase of the transition, however, the different time response is observed between the profiles near X- and O-points.

1. Introduction

Heliotron J [1,2] is a flexible helical-axis heliotron device with an $L = 1/M = 4$ helical coil ($\langle R_0 \rangle = 1.2$ m, $B_0 \leqslant 1.5$ T) based on the helical-axis heliotron concept [3]. One of the objectives of the Heliotron J experiments is to extend the understanding of the roles of edge plasma control in the omnigeneous (quasi-isodynamic) optimization scenario for this concept. In heliotron/stellarator devices the edge rotational transform $\iota(a)/2\pi$ is closely related with the edge field topology and the shape of the last closed flux surface (LCFS). In the standard configuration of Heliotron J, for example, there are seven "points" like the X-point of a tokamak divertor (see Fig. 1) [4] since $\iota(a)/2\pi \approx 0.56$ is close to the resonance condition of $n/m = 4/7$. Here n and m are the toroidal and poloidal mode numbers, respectively. Since this type of the edge field topology is commonly observed in advanced heliotrons/stellarator devices, it is important to investigate and understand the edge plasma characteristics in such a field topology.

In this study the edge plasma behavior near the X-point and O-point (a position between two adjacent X-points) has been investigated mainly with three movable Langmuir probes installed at three different positions in Heliotron J; outboard O-point, inboard and outboard X-points.

2. Experiment

In Heliotron J, the edge plasma behavior has been studied with a SOL-probe [5], divertor-probes [6] and also with fast cameras [7]. Recently, two more sets of movable Langmuir probes have been installed to investigate the edge plasma at different poloidal positions in one helical field pitch. Fig. 1 schematically shows the scanning line of the probe with vacuum magnetic surfaces and the puncture plots of edge magnetic fields at (a) #11.5, (b) #8.5 and (c) #7.5 sections. The Probe-#11.5 scans the plasma edge near an outboard O-point. Probe-#8.5 and Probe-#11.5 scan near inboard and outboard X-points, respectively. With these probes, the time evolution of the ion-saturation current I_s is monitored. The surface area of an electrode calculated by the mechanical dimension for #7.5, #8.5 and #11.5 probes are about 4 mm^2, 35 mm^2 and 21 mm^2, respectively. It is not easy, however, to estimate the effective collecting area of each probe in the magnetic field. The incidence angle of the field lines to the collecting surface of the electrode depends on the probe position. In this study we discuss the relative differences in the time behavior and/or spatial profile of I_s.

In this paper we focused on plasma initiated and maintained only by 2X-ECH (70 GHz, ~0.3 MW). To obtain the spatial profile, the positions of those probes were changed by shot-by-shot basis.

* Corresponding author.
E-mail address: mizuuchi@iae.kyoto-u.ac.jp (T. Mizuuchi).

0022-3115/$ - see front matter © 2009 Elsevier B.V. All rights reserved.
doi:10.1016/j.jnucmat.2009.01.116

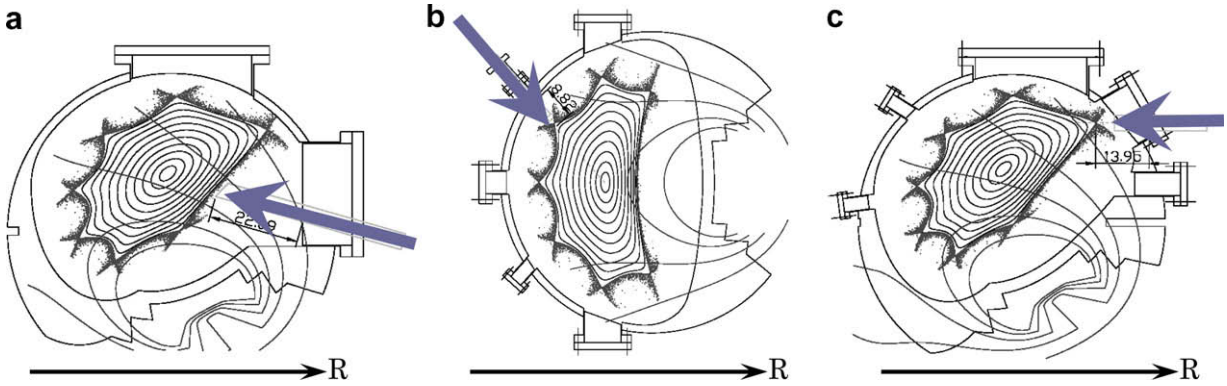

Fig. 1. Probe scanning-line for each probe section, (a) #11.5, (b) #8.5 and (c) #7.5. The flux surfaces, mod-B surface and the puncture plots of the edge magnetic filed lines are also plotted.

3. Experimental results and discussions

Fig. 2 shows an example of the time traces of the stored energy (W_p^{dia}), line-averaged density ($\bar{n}_e$), Hα intensity ($H_\alpha^{\#3.5}$) monitored at #3.5-section, 180° toroidally apart from #11.5, and ion-saturation currents at three positions, $I_s^{\#7.5}$, $I_s^{\#8.5}$ and $I_s^{\#11.5}$, respectively. The line of sight of the Hα monitor is almost a parallel one crossing the magnetic axis. In this study we focused on the edge plasma profile. To eliminate the effects of plasma fluctuations, the data in this figure are smoothed by a 5-kHz low-pass filter. The distance from LCFS along the scanning-path in the vacuum condition is denoted by ΔL, where negative value means the probe is inserted into the confinement region across LCFS. The data for the ECH-pulse and gas-puff are also plotted in the top two figures. The ECH with almost constant injection power was activated during 0.165–0.284 s. The density was controlled by the pre-programmed gas-puff. From the initial phase of the discharge, $\bar{n}_e$ gradually increases but seems to stop its increase around $t = T1$ (~0.23 s in this shot). Since the gas-puff rate is slightly decreased just before this timing, the stop of $\bar{n}_e$-increase might be related to the decrease of fueling rate. However, the intensity of $H_\alpha^{\#3.5}$ still continues to increase or keeps almost the same level as that for $t < T1$ and some MHD modes are observed around this timing. Therefore it should be careful to exclude the possibility of confinement degradation due to the MHD activities. At $t = T2$ ($>T1$), $H_\alpha^{\#3.5}$ starts to gradually decrease although the fueling rate is kept constant. Simultaneously W_p^{dia} and $\bar{n}_e$ starts to increase. These observations indicate the start of transition to the improved confinement mode reported in [8]. At $t = T3$ the increasing rate of $\bar{n}_e$ and W_p^{dia} goes up while the decreasing of $H_\alpha^{\#3.5}$ is accelerated (or $H_\alpha^{\#3.5}$ shows rapid drop). At $t = T4$, about 5 ms after $T3$ in this discharge, W_p^{dia} turns to decrease and $H_\alpha^{\#3.5}$ goes back to increase while $\bar{n}_e$ still keeps increasing, indicating the start of the radiation collapse. Corresponding to these events observed in Hα and the core plasma parameters ($\bar{n}_e$ and W_p^{dia}), some characteristic behaviors are observed in $I_s^{\#7.5}$, $I_s^{\#8.5}$ and $I_s^{\#11.5}$. In the particular discharge shown in Fig. 2, $I_s^{\#8.5}$ starts to decrease slightly at $t \sim T1$ while $I_s^{\#7.5}$ and $I_s^{\#11.5}$ still keep increasing. At $t \approx T3$, all I_s in this figure shows rapid drop and the low-I_s state continues until $t \approx T4$. After $t \approx T4$, $I_s^{\#7.5}$ and $I_s^{\#8.5}$ rapidly increase but $I_s^{\#11.5}$ stays at the low value. In this study it is found that these characteristic behaviors of I_s strongly depends on ΔL.

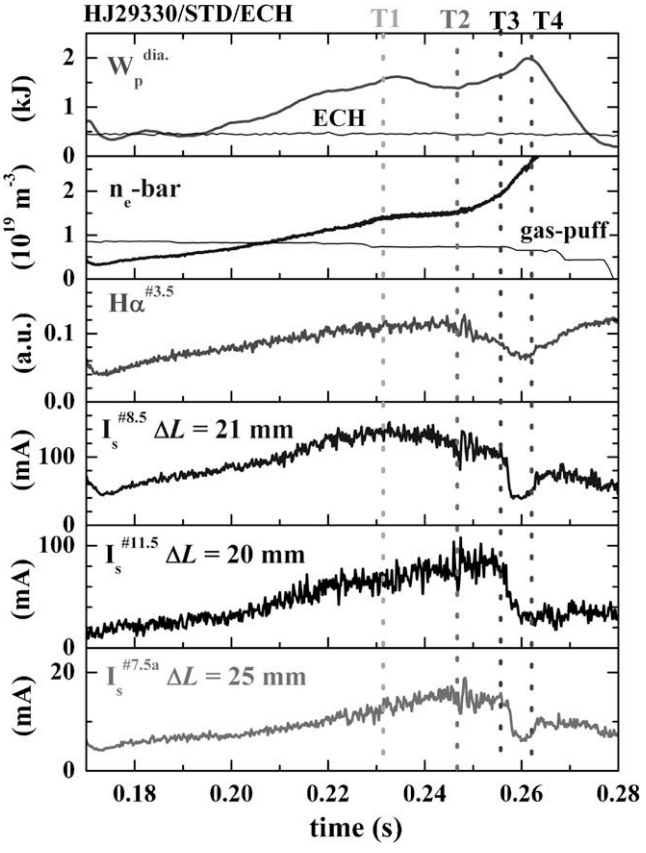

Fig. 2. A typical example of the time traces of the stored energy (W_p^{dia}), line-averaged density ($\bar{n}_e$), Hα intensity at the 3.5-section ($H_\alpha^{\#3.5}$) and ion-saturation currents at the three positions, $I_s^{\#8.5}$, $I_s^{\#11.5}$ and $I_s^{\#7.5}$.

Fig. 3 shows the time traces of (a) $I_s^{\#11.5}$, (b) $I_s^{\#8.5}$ and (c) $I_s^{\#7.5}$ with $H_\alpha^{\#3.5}$ for several ΔL. Since ΔL was changed by shot-by-shot basis, the reproducibility of the discharge is an important factor to analyze the dataset. In this study, some probes were inserted to the confinement region across LCFS for some shots. Probably due to such deep insertion of the probe, the reproducibility was not so excellent but the same time sequence of the concerned events was always observed for all the dataset although the absolute time for each event was not the same among the dataset. The scattering range of $\bar{n}_e$ and W_p at each timing is about (±20–30%).

As shown in Fig. 3, the time evolution of I_s in all three sections depends on ΔL. Focusing on the time span of $T3 < t < T4$, we can find a critical distance ΔL_{cr}^{T3-T4}. The ion-saturation current raises up during this period for $\Delta L < \Delta L_{cr}^{T3-T4}$, although it drops down for $\Delta L > \Delta L_{cr}^{T3-T4}$. For Probes-#11.5, -#8.5 and -#7.5, ΔL_{cr}^{T3-T4} s are ~16 mm, −8 mm (This position corresponds to $\rho \approx 0.98$ for the vacuum condition.) and −10 mm ($\rho \approx 0.98$), respectively. For the period of $T2 < t < T3$, there is another critical distance ΔL_{cr}^{T2-T3} for $I_s^{\#11.5}$ and $I_s^{\#7.5}$. While $H_\alpha^{\#3.5}$ gradually decreases in this period

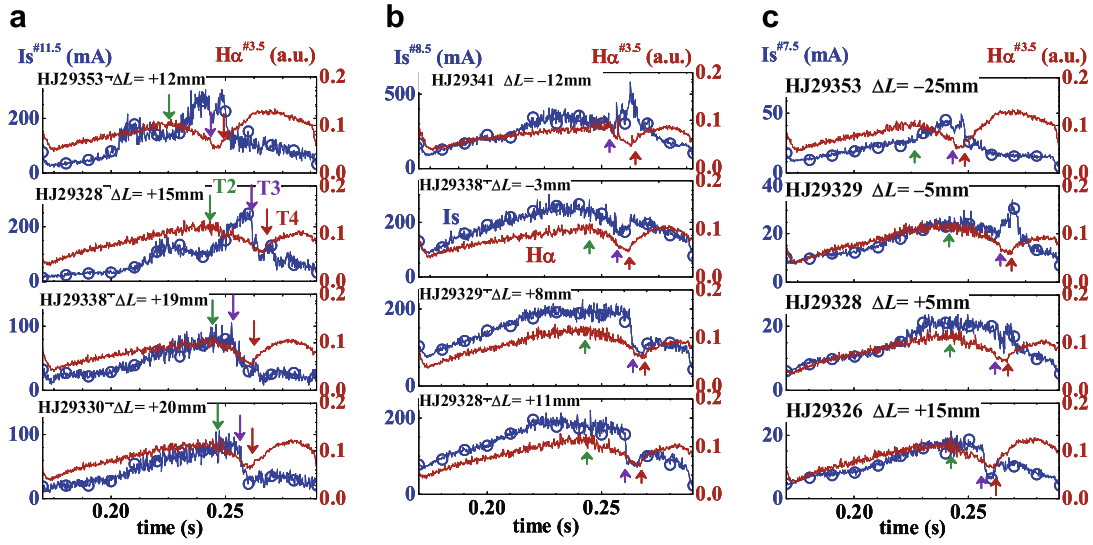

Fig. 3. Time trace of I_s for several ΔL. (a) $I_s^{\#11.5}$, (b) $I_s^{\#8.5}$ and (c) $I_s^{\#7.5}$ with the intensity of $H_\alpha^{\#3.5}$. Short arrows in the figures indicate the event timing T2, T3 and T4, respectively.

(Fig. 2), for $\Delta L < \Delta L_{cr}^{T2-T3}$, $I_s^{\#11.5}$ and $I_s^{\#7.5}$ clearly increase. For $\Delta L > \Delta L_{cr}^{T2-T3}$, however, almost the same value of $I_s^{\#11.5}$ ($I_s^{\#7.5}$) was kept or slightly decreased (increased) until $t \approx T3$. In this case, ΔL_{cr}^{T2-T3} is about 20 mm for Probe-#11.5 and about −20 mm ($\rho \approx 0.95$) for Probe-#7.5. The critical distance ΔL_{cr}^{T2-T3} for Probe-#7.5 is more core side than ΔL_{cr}^{T3-T4}, while ΔL_{cr}^{T2-T3} for Probe-#11.5 is more outer than ΔL_{cr}^{T3-T4}. On the other hand, $I_s^{\#8.5}$ is almost constant or decreases during this period at least for examined range of ΔL and no clear critical distance is observed for this time span.

The observed ΔL-dependence of the time behavior indicates that the spatial profile changes as the progress of the transition. Fig. 4(a–c) show the spatial profile of I_s for each probe at three timing as a function of ΔL, (a) $I_s^{\#11.5}$ (ΔL), (b) $I_s^{\#8.5}$ (ΔL) and (c) $I_s^{\#7.5}$ (ΔL). Here I_s are averaged over 2 ms during each phase, $T_{\sim 2}$ (from T2 − 1 ms to T2 + 1 ms), T_{2-3} (from T3 − 5 ms to T3 − 3 ms) and T_{3-4} (from T4 − 4 ms to T4 − 2 ms). Probe-#8.5 and -#7.5 inserted into the confinement region across LCFS without intolerable damage to the plasma performance although Probe-#11.5 disturbed the plasma performance even in the condition of $\Delta L > 0$ and was hard to cross LCFS. The reason of such difference of disturbance by the probe insertion is not clear at present. It might be related the difference in the thickness of so-called the ergodic field-line region and/or the interval between magnetic surfaces, which is wider near the X-point compared to that near the O-point as shown in Fig. 1. To discuss the difference in the absolute value of SOL plasma thickness at each probe section, it should be consider such difference of the field structure. It is possible to normalize with ρ for the confinement region but this technique does not work for the region outside LCFS. Moreover it should be noted that the plasma pressure and non-inductive plasma current can change the field topology including the spatial shift of LCFS from those in the vacuum condition [9]. Although the plasma pressure is low enough in this experiment to neglect its effect on the rotational transform profile, the non-inductive plasma current (<1 kA) increases the rotational transform and can deform slightly the edge field topology. To discuss the detailed deformation due to the plasma current, we need the current profile data. Since we have no such data at present, we use the field topology in the vacuum condition in this paper. In Fig. 4, the value of ρ for the vacuum condition is also shown for #7.5 and #8.5 sections. Fig. 5 shows the connection length profile along the probes' scan path in the vacuum condition. For the probes near the X-point, the connection length profile has a "flat part" due to the effect of the "fish-tail" part of the field topology. As shown in this figure, the difference in the radial position seems to be qualitatively understood by the difference in the connection length profile.

As shown in Fig. 4, it is found some common features of the profile change; (1) the profile becomes steeper as progress of the transition to the improved mode, (2) the clear decrease in outer part of measured region contributes to this steepening and (3) the change of I_s is not large in the inner part of the measured region during the transition although $\bar{n}_e$ rapidly increases. This suggests the reduction of diffusion takes place in more inner region. On the other hand, some peculiarities at each probe are also found. In early phase of the transition (T2−T3), near the outboard O-point, increase of $I_s^{\#11.5}$ is observed for $\Delta L < \Delta L_{cr}^{T2-T3}$ as discussed above and resulting steep gradient for the region of $\Delta L > 17$ mm. This increase seems to be swept out at the beginning of the later phase of the transition (T3−T4). On the other hand the spatial profiles by both the X-point probes keep their profiles in this phase. For the X-point probes, the $I_s^{\#8.5}$-profile has a deflection point of the profile at $\Delta L \sim -8$ mm and that for $I_s^{\#7.5}$-profile seems to be $\Delta L \sim 0$ mm.

4. Summary

The edge plasma profile (I_s-profile) and its time evolution at three different positions of the edge field topology (near inboard X-point, outboard O- and X-points) are compared focusing on the spontaneous change of the discharge mode to an improved confinement state in Heliotron J ECH plasma. In the early phase of the transition, Hα-emission gradually decreases while $\bar{n}_e$ and W_p^{dia} increase. The later phase is characterized by rapid drops of Hα and faster increases of $\bar{n}_e$ and W_p^{dia}.

For all three positions, it is found that (1) the profile becomes steeper as progress of the transition and (2) the decrease of I_s in outer part of SOL region contributes to this steepening. In the early phase of the transition, however, the different time response is observed between the profiles near X- and O-points; only the ion saturation current measured near the outboard O-point increases for the region inside a critical distance from LCFS. This increase seems to be swept out at the beginning of the later phase of the transition.

More careful studies on the locality of edge plasma response during the transition period to the improved confinement mode

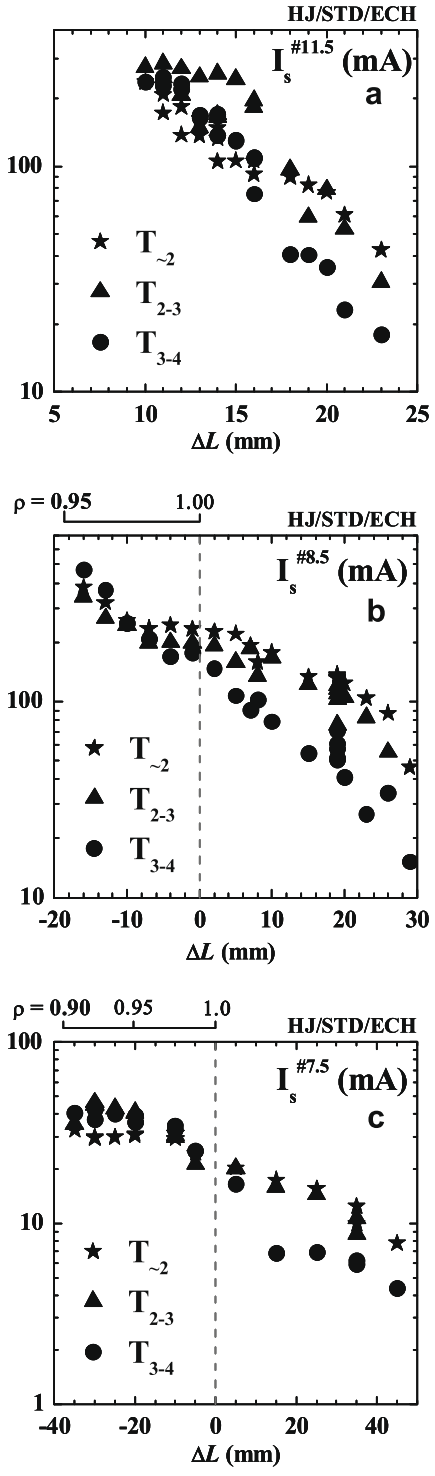

Fig. 4. Spatial profile of I_s at three timing ($T_{\sim 2}$, T_{2-3} and T_{3-4}) as a function of ΔL, (a) $I_s^{\#11.5}$ (ΔL), (b) $I_s^{\#8.5}$ (ΔL) and (c) $I_s^{\#7.5}$ (ΔL).

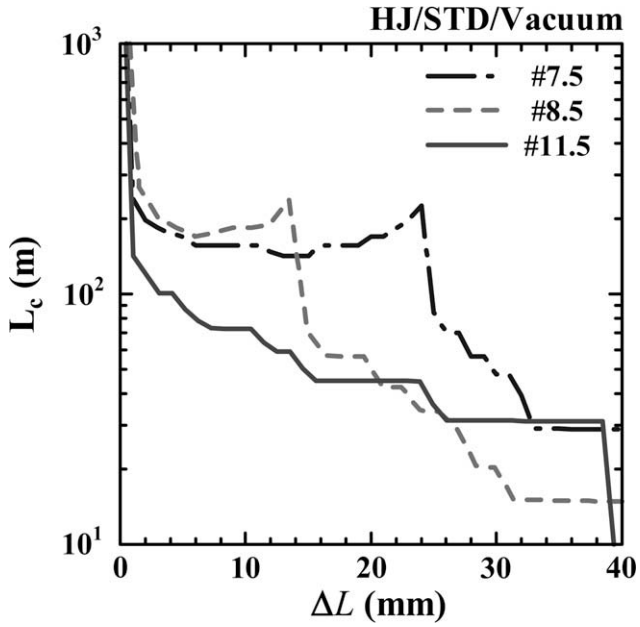

Fig. 5. Connection length profile along the probe path in the vacuum condition. $\Delta L = 0$ means the position of the last closed flux surface.

will be necessary to understand the mechanism of this observation in helical plasmas.

Acknowledgements

The authors are grateful to the Heliotron J supporting group for their excellent arrangement of the experiments. They also express their gratitude to Drs. S. Konoshima and K. Nagaoka for valuable discussions. This work is performed with the support and under the auspices of the Collaboration Program of the Lab. for Complex Energy Processes, IAE, Kyoto Univ., the NIFS Collaborative Research Program (NIFS04KUHL005, NIFS04-KUHL006, NIFS06KUHL010, NIFS07KUHL011, NIFS07KUHL015, NIFS04KUHL004 and NIFS04KUHL003) and the Grant-in-Aid of the Ministry of Education, Culture, Sports, Science and Technology of Japan (19560827).

References

[1] F. Sano et al., J. Plasma Fus. Res. Ser. 3 (2000) 26.
[2] T. Obiki et al., Nucl. Fus. 41 (2001) 833.
[3] M. Wakatani et al., Nucl. Fus. 40 (2000) 569.
[4] T. Mizuuchi et al., J. Plasma Fus. Res. Ser. 3 (2000) 192.
[5] T. Mizuuchi et al., J. Nucl. Mater. 337–339 (2005) 332.
[6] T. Mizuuchi et al., J. Nucl. Mater. 313-316 (2003) 947.
[7] N. Nishino et al., Plasma Fus. Res. 2 (2007) S1055.
[8] F. Sano et al., Nucl. Fus. 45 (2005) 1557.
[9] T. Mizuuchi et al., Nucl. Fus. 47 (2007) 395.